The structural dynamics of macropinosome formation and PI3-kinase-mediated sealing revealed by lattice light sheet microscopy

Shayne E. Quinn[1,2], Lu Huang[3,4], Jason G. Kerkvliet[4,5], Joel A. Swanson[6], Steve Smith[1,2], Adam D. Hoppe[4,5], Robert B. Anderson[1,2], Natalie W. Thiex[3,4]* Brandon L. Scott[1,2]*

1 South Dakota School of Mines and Technology (South Dakota Mines), Nanoscience and Nanoengineering, Rapid City, SD. 2 BioSNTR, South Dakota Mines, Rapid City, SD. 3 South Dakota State University (SDSU), Department of Biology and Microbiology, Brookings, SD. 4 BioSNTR, SDSU, Brookings, SD. 5 SDSU, Department of Chemistry and Biochemistry, Brookings, SD.6 University of Michigan, Department of Microbiology and Immunology, Ann Arbor, MI.

* Co-corresponding authors: natalie.thiex@sdstate.edu, brandon.scott@sdsmt.edu

Abstract

Macropinosomes are formed by shaping actin-rich plasma membrane ruffles into large intracellular organelles in a phosphatidylinositol 3-kinase (PI3K)-coordinated manner. Here, we utilize lattice lightsheet microscopy and image visualization methods to map the three-dimensional structure and dynamics of macropinosome formation relative to PI3K activity. We show that multiple ruffling morphologies produce macropinosomes and that the majority form through collisions of adjacent PI3K-rich ruffles. By combining multiple volumetric representations of the plasma membrane structure and PI3K products, we show that PI3K activity begins early throughout the entire ruffle volume and continues to increase until peak activity concentrates at the base of the ruffle after the macropinosome closes. Additionally, areas of the plasma membrane rich in ruffling had increased PI3K activity and produced many macropinosomes of various sizes. Pharmacologic inhibition of PI3K activity had little effect on the rate and morphology of membrane ruffling, demonstrating that early production of 3'-phosphoinositides within ruffles plays a minor role in regulating their morphology. However, 3'-phosphoinositides are critical for the fusogenic activity that seals ruffles into macropinosomes. Taken together, these data indicate that local PI3K activity is amplified in ruffles and serves as a priming mechanism for closure and sealing of ruffles into macropinosomes.

Introduction

Macropinocytosis, or "cell drinking," is a form of clathrin-independent endocytosis that results in the non-specific uptake of large volumes of extracellular fluid and solutes. This central macrophage function enables immune surveillance, clearing of debris, and sampling of the local environment for the presence of pathogen- or damage-associated molecular patterns, cytokines, growth factors, nutrients, and other soluble cues[1-6]. Macropinosomes also serve as platforms to integrate this diverse information and to activate a variety of signaling pathways[7-10]. The major macrophage growth factor, colony-stimulating factor-1 (CSF-1), stimulates macropinocytosis and contributes to ligand-dependent modulation of CSF-1 receptor signaling[9]. Additionally, cytokines such as CXCL12, and the bacterial cell wall component lipopolysaccharide (LPS) acutely stimulate macropinocytosis[5,11,12].

Construction of a macropinosome proceeds through autonomous, ligand-independent plasma membrane extensions known as ruffles, which are driven by actin polymerization and require the phosphorylation and dephosphorylation of different signaling phospholipids[2,13]. In the closely related process of solid particle uptake, the shape of the particle is used to template the phagosome structure[14,15]. In contrast, ruffles that fuse into macropinosomes do not have a structural framework to use as a template resulting in various potential closing mechanisms including 'purse string' closure of circular dorsal ruffles[13], closure at the distal tips of ruffles[7], and more recently described closure following actin tentpole crossing[12]. Regardless, the result is an internal organelle derived from the plasma membrane that is filled with extracellular fluid[16].

The dynamic lipid microenvironment impacts the localization of downstream effector molecules that drives actin polymerization and ruffle growth into macropinosomes[17]. The production of 3'

phosphoinositides by PI 3-kinase (PI3K) is required to generate isolated patches of phosphatidylinositol 3,4,5,triphosphate (PIP_3) on the plasma membrane[18,19], and the sequential breakdown of PIP_3 into $PI(3,4)P_2$ and ultimately PI is necessary for successful macropinosome formation[20]. It is only in the cellular slime mold *Dictyostelium,* that the signal coordination throughout the 3D ruffle volume during macropinocytosis has been well described[18], and there is still more to learn about how these events are spatially coordinated in metazoan cells[21]. The precise membrane dynamics of macropinocytosis and the spatial coordination of PI3K in forming ruffles remains unclear because of the low spatial and temporal resolution of other microscopy approaches. Previously, widefield ratiometric imaging has shown that PIP_3 concentration peaks after ruffle circularization[17,22,23], and PI3K inhibitors, including LY294002, have demonstrated that PI3K activity is only required for macropinosome closure, but does not inhibit ruffling[17]. Recently, high-resolution imaging of macropinocytosis in a macrophage-like cell line (RAW 264.7) indicated that the prior models of macropinocytosis may be more diverse than previously thought[12]. With the variety of different macrophage-like cell lines available, all of which perform constitutive macropinocytosis while displaying different phenotypes and protein expressions[24], it is more important than ever to expand the 3D understanding of membrane dynamics and protein localization during macropinocytosis.

Here, we employ the powerful three-dimensional (3D) imaging capabilities of lattice lightsheet microscopy[25] (LLSM) and volumetric image analysis to create high-resolution movies of plasma membrane dynamics and PI3K activity during ruffling and macropinocytosis. The images and movies we present advance our understanding of the spatial dynamics of membrane ruffling, the morphologies that lead to macropinosomes, the spatial distribution of PI3K activity during macropinocytosis, and finally acknowledge the structural variability among different cell lines during macropinocytosis in fetal liver (FLM), bone marrow derived (BMDM), and RAW 264.7 macrophages. Our results show that the majority of macropinosomes form by non-specific collisions of adjacent PI3K-rich ruffles. We show that PI3K activity is present at the earliest stages of ruffle extensions and is highly localized to the bottom of ruffles after the membrane has closed into a macropinosome. Finally, we modulate the rate of macropinocytosis using stimulation and pharmacological inhibition to demonstrate that the ruffle morphology is unaffected, but PI3K activity is required to prime ruffle membranes for sealing into macropinosomes.

Results

LLSM allows volumetric visualization of plasma membrane movements relative to PIP_3 and $PI(3,4)P_2$ distribution during macropinocytosis

Our first objective was to capture the 3D structure of the plasma membrane relative to PI3K activity during macropinosome formation. LLSM imaging was performed on fetal liver macrophages (FLMs) stably expressing the fluorescent proteins mNeonGreen localized to the plasma membrane via the lipidation signal sequence from Lck (Mem-mNG) and the pleckstrin homology domain of Akt fused to mScarlet-I (AktPH-mSc). The AktPH probe recognizes PIP_3 and $PI(3,4)P_2$ with similar affinity and has been used extensively to characterize PI3K activity during macropinocytosis[8]. Using LLSM imaging in conjunction with the molecular visualization software, ChimeraX[26], we represent the data using the following renderings: isosurface, surface mesh, volumetric maximum intensity, and orthogonal planes. An isosurface is a three-

89 dimensional contour map that represents points in volume space as constant values at a given intensity
90 threshold causing all pixels above the threshold to be shown as a solid-colored voxel (value of 1), while all
91 voxels below the threshold are transparent/hidden (value of 0) resulting in a crisp surface depiction of the
92 membrane probe (Fig. 1a). These images were of sufficient resolution that the detailed structure of ruffles
93 and forming macropinosomes could be observed in living cells (Fig. 1a), similar to scanning electron
94 microscopy imaging of bone marrow derived macrophages (Fig. 1b). The isosurface is rendered with
95 ambient occlusions meaning that any internal information is hidden from view. To visualize the
96 recruitment of AktPH-mSc relative to the membrane, we first used volumetric intensity renderings that
97 display the most intense color value underlying the pixel along the line of sight (ChimeraX User Guide),
98 which provides a visually intuitive method of displaying 3D fluorescent intensities (Fig. 1c). The resulting
99 volume is similar to a maximum intensity projection; however, the projection dimension is dependent on
100 the orientation, i.e., top down would yield an xy-maximum intensity projection collapsed in z and a side
101 view would provide the corresponding xz/yz maximum intensity collapsed in y/x respectively. As can be
102 seen in the volume renderings, Mem-mNG persisted on newly formed intracellular vesicles derived from
103 the plasma membrane (Fig. 1c). Moreover, we observed membrane movements throughout the entire
104 formation and early trafficking of macropinosomes, as well as the recruitment of AktPH-mSc to forming
105 macropinosomes (Fig. 1c (arrow), Supplementary Movie 1). It is difficult to perceive depth in the still-
106 frame volumetric renderings but orthogonal plane slices (orthoplanes) in xy, yz, and xz (~0.1 µm thick)
107 showed that AktPH-mSc was enriched in ruffles to varying degrees and intensely labeled circular
108 structures found near the base and sides of ruffles (Fig. 1d, Supplementary Movie 2). While orthoplanes
109 are effective for examining the 2D relationships between the fluorescent signals, they can also produce
110 incomplete or distorted perspectives that are resolved by viewing the full volumetric data (Supplementary
111 Figure 1), such as when a macropinosome appears closed vs open. To overcome these limitations, we
112 implemented a mesh derived from the Mem-mNG isosurface with transparent polygonal faces (only
113 displaying edges and vertices) that enables visualizing the underlying volumetric AktPH-mSc signals, while
114 maintaining the structural framing needed to resolve plasma membrane rearrangements (Fig. 1e).

115 For visualizing a macropinosome sealing event, we began by imaging a representative cell for these data
116 that retained the canonical morphology like that of BMDMs with a profile view representing a 'fried egg'
117 ranging from ~1 µm thick at the outer edge and up to ~6 µm thick near the center. Next, an XY-MIP was
118 used to quickly find potential closures using the AktPH-mSc signal as an indicator. The identified
119 coordinate was then translated to the corresponding isosurface, and the timepoint at which the isosurface
120 was fully closed was considered as a nascent macropinosome. These formations were examined using the
121 full volumetric intensity projections for further analysis. Together, combinations of these visualization
122 techniques were applied to 122 macropinosome formations and enabled correlating the location and
123 timing of PI3K activity to the membrane extension, curvature, and fusion of macropinosomes with
124 unprecedented spatial and temporal resolution.
125

126 **AktPH-mSc is recruited early during ruffle expansion and peaks at the base of ruffles after**
127 **macropinosome sealing**

128 In prior analysis of macropinocytosis using microscopy methods with low axial resolution, AktPH
129 recruitment was identified as ruffles that transitioned into closed circular ruffles and nascent

macropinosomes[8]. Here, the enhanced z-axis resolution and detection sensitivity of LLSM enabled visualizing the dynamic recruitment of AktPH-mSc to ruffles as they began to protrude from the plasma membrane (Fig. 2a) until maturation where tubulation and fusion between adjacent macropinosomes occurs (Supplementary Movie 3). As these early ruffles expanded laterally along the plasma membrane and protruded vertically from the cell surface, some ruffles continued to accumulate AktPH-mSc, whereas others lost AktPH-mSc and receded back into the cell suggesting different levels of PI3K activity in neighboring ruffles influences the outcome of a ruffling region (Fig. 2b). Ruffles that maintained AktPH-mSc throughout the ruffle volume continued to grow and formed macropinosomes, which were accompanied by an intense transient recruitment of AktPH-mSc to the base of the ruffle around the nascent macropinosome (Fig. 2c, Supplementary Movie 4). Given the early localization and amplification of PI3K signaling in ruffles that become macropinosomes, we wondered in what ways PI3K activity contributed to 3D ruffle dynamics.

PI3K activity is required for macropinosome sealing, but not ruffling

To gain insight into the role of PI3K in regulating the morphological dynamics of macropinocytosis, we used the broad-spectrum PI3K inhibitor LY294002, which inhibits the closure phase of macropinocytosis in macrophages[27]. Non-treated control cells formed transient dorsal ruffles that recruited AktPH-mSc and closed into macropinosomes, as seen by the surface rendering and intracellular void that is maintained in the plane view (Fig. 3a-c, Supplementary Movie 5). LY294002 treatment for 30 min did not stop ruffle formation, but eliminated AktPH-mSc recruitment to membrane ruffles (Fig. 3d,e, Supplementary Movie 6). Furthermore, LY294002-treated cells formed ruffles that appeared to close into a macropinosome but retracted back to the plasma membrane and failed to maintain an intracellular organelle (Fig. 3f). In order to further understand the dynamic cellular response to PI3K inhibition, we imaged the same cells immediately before and after LY294002 treatment. Immediately after treatment, PI3K activity was halted as evidenced by clearance of AktPH-mSc from the PM ruffles and diffuse cytosolic localization (Supplementary Figure 2). Interestingly, many of the ruffles receded into the plasma membrane, but ruffling resumed within 10 min and was similar to the untreated cells by 30 min (Supplementary Movie 7). Taken together, these data suggest that PI3K activity is dispensable for ruffle formation but is required for membrane sealing to generate a macropinosome.

PI3K activity primes ruffles for fusion to seal into nascent macropinosomes

We next sought to categorize the macropinosome formation based on the way the membrane fused and the relative amount of PI3K activity. Based on the previously established models for macropinosome formation there would be distinguishing characteristics depending on the sealing formation method. Either we would find linear extensions where the distal tips would collide, circularize, and seal, or we would find filopodial spikes that form and the membrane would fill in the space between before twisting to seal[12]. Surprisingly, we found that approximately 88% of the quantified macropinosomes formed when the leading edge of extending ruffles collided along the sides of nearby membrane surface or ruffles that typically only involved a small portion of the second ruffle, so long as the ruffle area had elevated AktPH-mSc (Fig. 4). The remaining 12% of events we observed were classified as tidal-wave like structures in which a mostly isolated planar ruffle extended from the cell surface where the entire ruffle was rich in AktPH-mSc, the ruffle gained curvature in a rolling fashion, and resulted in fusing back with the plasma

170 membrane rather than an extending ruffle (Supplementary Movie 5). However, given that the entire ruffle
171 area was rich in AktPH-mSc, these types of formation follow the same underlying mechanism as collisions
172 with adjacent membrane extensions. Frequently, a single ruffle area produced multiple macropinosomes
173 and were the result of similar but smaller ruffle extensions that quickly fused near the base of larger ruffles
174 (Fig. 4). Within the ruffle, forming macropinosomes recruited AktPH-mSc near the base of the ruffle as
175 they transitioned into a spherical shape prior to detaching from the plasma membrane and moving
176 independently (Fig. 4, Supplementary Movies 3,8). We hypothesized that regions with highly concentrated
177 AktPH-mSc localization would correlate with increased macropinocytic activity. Indeed, this phenomenon
178 was observed in four of the eleven constitutive cells (Fig. 5). These ruffling regions resulted in the
179 formation of many macropinosomes through the intersection of multiple ruffles that were nearly
180 indistinguishable from one another and only became apparent through the PI3K post closure activity (Fig.
181 5d,e). Therefore, the elevated PI3K activity creates a microenvironment suited for the rapid fusion of PI3K-
182 primed ruffles into macropinosomes of various sizes within short timeframes (Supplementary Movies
183 9,10). We hypothesized that other signaling that activates PI3K activity may stimulate distinct ruffling
184 morphologies or modulate the rate of macropinocytosis.

185 **CSF-1 growth factor signaling promotes extensive circular ruffling and macropinocytosis**

186 CSF-1 is an essential macrophage growth factor that stimulates macropinocytosis at levels controlled by
187 the concentration of the CSF-1 signal[9]. Macrophages starved of CSF-1 for 24 hrs and then acutely
188 stimulated produced expansive circular ruffles that initiated from the distal cellular margins coincident
189 with cellular spreading (Fig. 6). LLSM imaging revealed a circular ruffle that initiated at the edge of the cell
190 with a height of approximately 2 µm above the dorsal surface and constricted to a central location in a
191 coordinated manner (Fig. 6a). A striking feature of this ruffle was the confinement of AktPH-mSc within
192 the limiting edge of the ruffle. As the circular ruffle constricted toward the center of the cell, AktPH-mSc
193 was highly concentrated within it and was nearly undetectable in the rest of the cell (Fig. 6b,
194 Supplementary Movie 11). In the volumetric projections, many macropinosomes were observed to form
195 during the constriction process without additional membrane protrusions being generated. This is
196 consistent with our hypothesis that increased PI3K activity primes membranes for fusion to generate
197 macropinosomes (Fig. 6c, Supplementary Movies 11,12). Thus, CSF-1 initiated long range signaling and
198 PI3K activation resulting in coordinated movements of the cytoskeleton throughout the cell.

199 **LPS stimulates regional ruffling and generates large numbers of macropinosomes**

200 The bacterial cell wall component lipopolysaccharide (LPS) activates PI3K through the Akt pathway[28], and
201 acutely stimulates macropinocytosis[3]. Recently, LPS stimulation was used to characterize a novel
202 formation mechanism involving actin tentpoles supporting membrane veils which cross to create a
203 macropinosome[12]. When FLMs were exposed to LPS, regional patches of membrane ruffling were
204 generated that migrated around the dorsal surface of the macrophage (Fig. 7a, Supplementary Movie 13)
205 in a manner distinct from the dorsal surface ruffle generated by CSF-1 stimulated cells (Fig. 6); however,
206 this process was similar in appearance to constitutive macropinocytosis (Fig. 7c, Supplementary Movie
207 14). The patches of ruffles in LPS-treated cells generated many small ruffles, had elevated PI3K activity
208 and were more efficient at forming macropinosomes as compared to control (Fig 7d). Thus, the nature of
209 macropinosome formation is coordinated over different length scales with differing intensities depending

210 on the nature of the activating stimulus. Regardless, PI3K activity delineates ruffles and regions of the
211 plasma membrane where macropinosomes form.

212 Discussion & Conclusion

213 Here, we have utilized lattice light sheet microscopy to develop a new level understanding of the
214 structural dynamics and PI3K signaling underpinning macropinocytosis. Until recently, dynamic processes
215 such as macropinocytosis were characterized using optical techniques with poor axial resolution and
216 elevated phototoxicity leading to subsampling the spatial and temporal dynamics and requiring inference
217 from multiple methods such as scanning electron microscopy of fixed cells to address the formation
218 mechanism of macropinosomes. Lightsheet microscopy overcomes these obstacles and enables us to
219 record, with sufficient spatial and temporal resolution, the complete evolution of membrane ruffles and
220 the mechanism by which these ruffles form into macropinosomes while also measuring the redistribution
221 of signaling molecules controlling these processes. We have shown that macropinosomes form through
222 several possible morphologies; however, in each case PI3K activity primes ruffles for fusion with adjacent
223 primed membranes to form macropinosomes. In areas with elevated PI3K activity, either naturally or
224 through external stimulation, there was an increased ruffle density leading to an increased probability of
225 primed ruffles colliding to form macropinosomes. This model of macropinosome formation relying on
226 PI3K priming rather than a defined geometry also explains the variation in diameter that is a hallmark of
227 macropinosomes. The improved sensitivity of LLSM enabled detection of PI3K activity at the earliest
228 stages of ruffle development that grows in curving ruffles and peaks around macropinosomes post
229 closure. Our data are consistent with a mechanism driven by the geometry of curving ruffles that confines
230 PI3K, thereby amplifying the signal, which in turn activates yet unknown fusogenic protein(s) localized to
231 the ruffle edges mediating sealing during membrane collisions. This conclusion is supported by the
232 observations that inhibition of PI3K activity with LY29004 did not substantially alter membrane ruffling
233 structure, curvature, or collisions but completely inhibited sealing, even when fully spherical
234 morphologies were observed that then collapsed back into the cell surface. These data are consistent with
235 previous work using LY294002 as a broad-spectrum PI3K inhibitor and the extensive work done on PI3-
236 kinase in dictyostelium[29,30]

237 The model suggested in this work contrasts with a recent report in LPS-activated RAW 264.7 cells that
238 described F-actin-rich filopodial "tentpoles" protruding from the surface that twisted to constrict veils of
239 membrane that then became macropinosomes[12]. Using Mem-mNG and Lifeact-mSc in RAW 264.7 cells
240 under identical imaging conditions, we observed filapodial extensions that fit with the tentpole formations
241 described previously (Supplementary Figure 3). However, we also transduced BMDM with the same NG-
242 membrane probe and found no tentpole like structures; rather the FLM and BMDM were similar in their
243 flat and smooth dorsal surfaces with large lamellar sheet-like ruffles (Supplementary Figure 3), suggesting
244 that the tentpole-like formation is dispensable for macropinocytosis and may be unique to the RAW264.7
245 cell line.

246 Our data demonstrate that macropinosomes form from a variety of morphologies in macrophages,
247 contrary to the morphologies in other cells such as the tightly controlled process observed in
248 Dictyostelium. Specifically, macropinocytosis in Dictyostelium appears to involve the formation of a cup

249 with a clearly segregated PIP3 containing domain[29] whereas, our observations as well as the work of
250 Condon et al using LLSM indicates that initiation of macropinosomes by macrophages arises from a
251 morphologically diverse and somewhat chaotic ruffling process. Importantly, the well-defined PIP3
252 containing domains observed in Dictyostelium appear similar to the macropinosomes in macrophages at
253 the sealing stage, in which substantial PIP3 products accumulate (Fig. 2). We speculate that these
254 differences are attributed to the importance of macropinocytosis in *Dictyostelium* as a method of nutrient
255 gathering[30,31], while macrophages perform constitutive macropinocytosis in order to sample the
256 environment for antigen presentation[2,7].

257 Taken together, our experiments indicate a mechanism for macropinosome formation requiring amplified
258 PI3K signaling within ruffles that become macropinosomes and that PI3K contributes primarily to priming
259 membranes for sealing. The membrane probe and visualizations we have described set the foundation to
260 enable rigorous testing of this mechanism using specific inhibitors and sensors that bind to the various
261 products to determine how each step is regulated during macropinocytosis.

262 Methods and Materials

263 **Plasmids.** pCMV-VSV-G was a gift from Bob Weinberg (Addgene plasmid #8454;
264 http://n2t.net/addgene:8454; RRID:Addgene_8454)[32]. psPAX2 was a gift from Didier Trono (Addgene
265 plasmid #12260; http://n2t.net/ addgene:12260; RRID:Addgene_12260). pLJM1-EGFP was a gift from
266 David Sabatini (Addgene plasmid #19319 ; http://n2t.net/addgene:19319 ; RRID:Addgene_19319)[33]. Lck-
267 mScarlet-I and Lifeact-mScarlet-I were gifts from Dorus Gadella (Addgene plasmids #98821, #85056;
268 http://n2t.net/addgene:98821; http://n2t.net/addgene:85056; RRID:Addgene_98821,
269 RRID:Addgene_85056)[34].

270 **Construction of the membrane and AktPH probes**. The membrane probe was constructed by combining
271 the membrane localization motif (MGCVCSSNPE) from Lck[34] in frame with mNeonGreen in the pLJM1
272 backbone containing the puromycin resistance gene. The AktPH-mSc probe was constructed by using the
273 pleckstrin homology domain from Akt in frame with mScarlet-I in the pLJM1 backbone, modified to
274 contain the blasticidin resistance gene. Sequences were codon optimized for expression in mouse cells,
275 synthesized, and sequence verified by GenScript (Piscataway, NJ).

276 **Viral transduction.** Sequence-verified plasmids containing genes encoding FP-chimeras, plus the
277 packaging plasmids pVSV-G and psPAX2 were transfected into NIH 293T cells for packaging using linear
278 25 kDa polyethylenimine (PEI) as a transfection reagent. NIH 293T-cell culture supernatant containing
279 lentiviral particles was collected and added to either BMDMs, RAW 264.7, or FLMs each treated with
280 cyclosporin A (10 µM) for two days. Transduced FLMs were selected with puromycin and blasticidin (10
281 $\mu g \cdot ml^{-1}$ each).

282 **Macrophage culture media**. DMEM/F-12 (Gibco) supplemented with 20% Heat-inactivated FBS (R&D
283 Systems), 1% Penicillin/Streptomycin (Gibco), 50 $ng \cdot ml^{-1}$ mCSF-1 (BioLegend), and 5 $\mu g \cdot ml^{-1}$ plasmocin
284 (Invivogen) maintained at 37°C with 7.5% CO_2.

285 **PIP_3 inhibition (LY294002).** Coverslips were prepared as described in 'Cell culturing and coverslip plating'
286 and moved to a well of media containing 50 µM LY294002 where it was incubated for 30 minutes at 37°C

287 and 7.5% CO_2 prior to imaging. The coverslip was then transferred to the LLSM bath containing Imaging
288 Media, 1.7 mM Glucose, and 50 µM LY294002. The coverslip was explored using the LLS software, and
289 three cells were chosen per coverslip that provided the best visual representation of the population. Each
290 cell was imaged under the same parameters as described in 'Lattice light sheet microscopy imaging'.
291 Additionally, coverslips were tested to ensure the 30 min treatment was sufficient by imaging a coverslip,
292 introducing LY294002 at 50 µM, and imaged three cells representing the full 30 minute treatment. Finally,
293 untreated coverslips were placed on the microscope and three cells were selected. The three cells were
294 imaged prior to drug treatment in the imaging bath then LY294002 was introduced at 50 µM and each cell
295 was reimaged in reverse order (1-2-3-3-2-1). Alongside these tests a DMSO control was performed to
296 further ensure the proper treatment.

297 **CSF-1 stimulation***.* The coverslip was starved overnight in DMEM/F-12 with 10% FBS and 1% pen/strep.
298 After 24 h the coverslip was moved to the LLS bath containing 7 mL L-15 imaging media, and 1.7mM
299 Glucose. The coverslip was explored using the LLS software and three cell targets were chosen and imaged
300 for a pre-stimulation comparison. Immediately after imaging the third cell, CSF-1 was introduced at 50 ng
301 $\cdot mL^{-1}$ to the 7 mL bath. The third cell was once again imaged < 1 min after stimulation and each additional
302 cell was imaged in reverse order (Imaging order 1-2-3-3-2-1).

303 **Lipopolysaccharide stimulation**. FLMs were stimulated with 100 $ng\cdot ml^{-1}$ Lipopolysaccharides from
304 *Salmonella enterica* serotype enteritidis (Sigma) for 24 h in culture media before being transferred to
305 imaging media containing 100 $ng\cdot ml^{-1}$ for LLSM experiments.

306 **Macrophage isolation**. Fetal liver macrophage (FLM) cell cultures were generated as described
307 previously[35,36]. Livers were isolated from gestational day 15-19 mouse fetuses from C57BL/6J mice (The
308 Jackson Laboratory, Bar Harbor, ME) in accordance with South Dakota State University Institutional
309 Animal Use and Care Committee. Liver tissue was mechanically dissociated using sterile fine-pointed
310 forceps and a single-cell suspension was created by passing the tissue through a 1 ml pipette tip[35]. Cells
311 were plated on non-tissue culture treated dishes and kept in growth and differentiation medium
312 containing the following: 20% heat-inactivated fetal bovine serum; 30% L-cell supernatant, a source of M-
313 CSF[37,38]; and 50% Dulbecco's modified growth medium containing 4.5 $g\cdot L^{-1}$ glucose, 110 mg L^{-1} sodium
314 pyruvate, 584 $mg\cdot L^{-1}$ L-glutamine, 1 IU ml^{-1} penicillin and 100 $\mu g\cdot ml^{-1}$ streptomycin. FLM were cultured for
315 at least 8 weeks prior to transduction and experiments.

316 **Cell Culturing and Coverslip Plating.** FLMs were cultured in T-25 tissue culture flasks using the following
317 culture media: DMEM F-12 with 20% FBS, 1% penicillin/streptomycin, 50 $ng\cdot ml^{-1}$ CSF-1, and 5 $ng\cdot ml^{-1}$
318 plasmocin. The cell cultures were split at ~85% confluence, first by washing the T-25 flask with 3 mL of
319 PBS (-Ca/-Mg) 2 times. The cells were then lifted from the T-25 flask using 4 mL of 4°C PBS (-Ca/-Mg,
320 +0.98mM EDTA) with gentle pipet washing for approximately 10 min. The lifted cells were moved to a 15
321 mL centrifuge tube (1 mL of culturing media was added to 15 mL tube if cells took >10 min to lift) and
322 centrifuged at 200 x g for 5min. While the cells were being spun down, the T-25 flask was washed with
323 PBS (-Ca/-Mg), filled with 5mL of culture media, and placed in the 37°C incubator to reach appropriate
324 culture conditions. Once the cells were finished being spun down, the supernatant was removed from the
325 15 mL tube and the cells were resuspended in 1 mL culturing media and counted. The counting was done
326 by mixing 10 µL of suspended cells with 10 µL of trypan blue and placed on a glass slip to be counted using

327 a countess. The FLMs were re-plated in the original T-25 flask with ~6-7 x 10^5 cells. The cells were washed
328 every 2 days and given fresh media until reaching ~85% confluence where they would then be split. Cell
329 lines were kept for approximately 2 months before being replaced with early state frozen aliquots.
330 Macrophages were prepared for LLS imaging 24 h prior to imaging using 5mm glass coverslips. The
331 coverslips were soaked in 90-100% ethanol and flame cleaned using a butane flame. Approximately 5
332 flame cleaned coverslips were placed per well of a 12 well plate each containing 1 mL of culture media.
333 Cells were added to each well during the cell culture process described above at ~3x10^5 cells to each
334 3.5cm^2 (12-well plate) for imaging. The FLMs incubated on the flame cleaned glass coverslips in culturing
335 media for 24 h prior to imaging. The coverslips were transferred to the LLSM bath that was filled with 7
336 mL of Leibovitz's L-15 Media (supplemented with 1.7 mM glucose) at ~37°C.

337 The RAW 264.7 macrophages were purchased from ATCC and maintained using the suggested subculture
338 routine. Briefly, cells were split between 70-80% confluence, reseeded at 2-4 x 10^4 cells cm^{-2}, and cultured
339 in DMEM F-12, requiring 7.5% CO_2 at 37°C. Due to the variability in adherence, cells were lifted using the
340 recommended cell scraper protocol. The same protocol as discussed above was used for plating cells for
341 imaging on the LLSM.

342 **Lattice Light Sheet Microscopy.** The LLSM is a replica of the design described by Chen et al.[25], built under
343 license from HHMI. Volumetric image stacks were generated using dithered square virtual lattices (Outer
344 NA 0.55, Inner NA 0.50, approximately 30 µm long) and stage scanning with 0.5 µm step sizes, resulting
345 in 254 nm deskewed z-steps. Excitation laser powers used were 18µW (488 nm) and 22µW (561 nm),
346 measured at the back aperture of the excitation objective. The emission filter cube (DFM1, Thorlabs)
347 comprised a quadband notch filter NF03-405/488/561/635 (Semrock), longpass dichroic mirror Di02-R561
348 (Semrock), shortpass filter 550SP (Omega) on the reflected path, and longpass filter BLP01-561R
349 (Semrock) on the transmitted path; the resulting fluorescence was imaged onto a pair of ORCA-Flash4.0
350 v2 sCMOS cameras (Hamamatsu). The camera on the reflected image path was mounted on a manual x-
351 y-z translation stage (Newport 462-XYZ stage, Thorlabs), and the images were registered using 0.1 µm
352 Fluoresbrite YG microspheres (Polysciences). The image capturing rates varied between 5-10 seconds per
353 volume using 8-12 ms planar exposures depending on the brightness of the cell and imaging region.

354 **Scanning Electron Microscopy.** BMDM were plated onto 13 mm diameter, circular glass coverslips and
355 cultured overnight in RPMI with 10% FBS (R10). To stimulate macropinocytosis, BMDM were incubated
356 30 min in phosphate-buffered saline (PBS), then 15 min in PBS containing 10 nM CSF-1. Cells were fixed in
357 2% glutaraldehyde, 0.1 M cacodylate buffer, pH 7.4, 6.8% sucrose, 60 min at 37 °C. Fixative was replaced
358 with a second fixative consisting of 1% OsO_4 in 0.1 M cacodylate buffer, pH 7.4, for 60 min at 23 °C. The
359 second fixative was replaced with 1% tannic acid in cacodylate buffer, 30 min at 4 °C, the rinsed with 3
360 changes of 0.1 M cacodylate buffer. Coverslips were transferred through successive changes of acetone-
361 water mixtures, progressively increasing acetone concentrations to 100% before a final incubation in
362 hydroxymethylsilazidane (HMDS, EM Sciences). HMDS was removed and coverslips were dried for 2 days.
363 Coverslips were shadowed with gold and observed on a Amray 1900 field emission scanning electron
364 microscope.
365 **Deconvolution and Post Processing.** The raw volumes acquired from the LLSM followed the standard
366 protocol including deskewing, deconvolving and rotating to coverslip coordinates in LLSpy[39] as the raw

367 data acquired from LLSM is captured at an approximate angle of ~32° with respect to the coverslip. We
368 applied a fixed background subtraction based on an average dark current image, 10 iterations of Lucy-
369 Richardson deconvolution with experimentally measured point spread functions for each excitation
370 followed by rotation to coverslip coordinates and cropping to the region of interest surrounding the
371 volume for visualization. We optimized the illumination for minimal photobleaching to occurred during
372 the experiments. The fully processed data was opened as a volume map series in UCSF ChimeraX and
373 utilized isosurface, mesh, 3D volumetric intensities, and orthogonal planes renderings to exam the data.
374 The surface and mesh options utilize a three-dimensional analog of an isoline called an isosurface that
375 represents points in volume space as constant values which were used to display the membrane probe.
376 The isosurface provides a defined surface for the membrane probe resulting in shadowing providing visual
377 depth to the three-dimensional data. The mesh rendering offers a similar surface definition while also
378 providing an option to include the internal fluorescent AktPH-mSc signal. We used a volumetric intensity
379 projection to visually display the localization of AktPH-mSc throughout the cell. The final technique used
380 to display the LLSM data was through orthogonal planes. This generates 2D planes each 0.128 µm thick
381 for the entire volume in xy, yz, and xz. Multiple methods were overlapped and shown side by side to
382 effectively represent the data and labeled within each figure. It is important to note that all fluorescent
383 information is retained within each individual pixel, providing a correlated visual increase with fluorescent
384 probe localization.

385 **Acknowledgments**

386 *Funding:* Funding provided by the South Dakota Board of Regents through BioSNTR and the SDBOR FY20
387 collaborative research award "IMAGEN: Biomaterials in South Dakota". Additional funding provided by the National
388 Science Foundation through research award CNS-1626579 "MRI: Development of a Scalable High-Performance
389 Computing System in Support of the Lattice Light-sheet Microscope for Real-time Three-dimensional Imaging of
390 Living Cells". J.A.S. was supported by NIH grant R35 GM131720. B.L.S. is supported by the Chan Zuckerberg Initiative
391 through the Imaging Scientist program.

392 *Visualization:* The data visualization and analyses were performed using UCSF ChimeraX, developed by the
393 Resource for Biocomputing, Visualization, and Informatics at the University of California, San Francisco, with support
394 from National Institutes of Health R01-GM129325 and the Office of Cyber Infrastructure and Computational Biology,
395 National Institute of Allergy and Infectious Diseases.

396 *LLSM:* The Lattice Light Sheet Microscope referenced in this research was developed under license from Howard
397 Hughes Medical Institute, Janelia Farms Research Campus ("Bessel Beam" patent applications 13/160,492 and
398 13/844,405).

399 *Author Contributions:* S.E.Q. acquired and analyzed LLSM data and co-wrote the manuscript. L.H generated FLM cell
400 lines used in experiments. J.G.K. Designed plasmid constructs and generated FLM cell lines. J.A.S. Performed SEM
401 experiments and edited the manuscript. S.S. provided supervision and edited the manuscript. A.D.H. co-wrote the
402 manuscript. R.B.A. built the LLSM and analysis cluster and provided supervision. N.W.T. designed experiments and
403 co-wrote the manuscript. B.L.S. designed and performed initial experiments, assisted with data analysis and co-
404 wrote the manuscript.

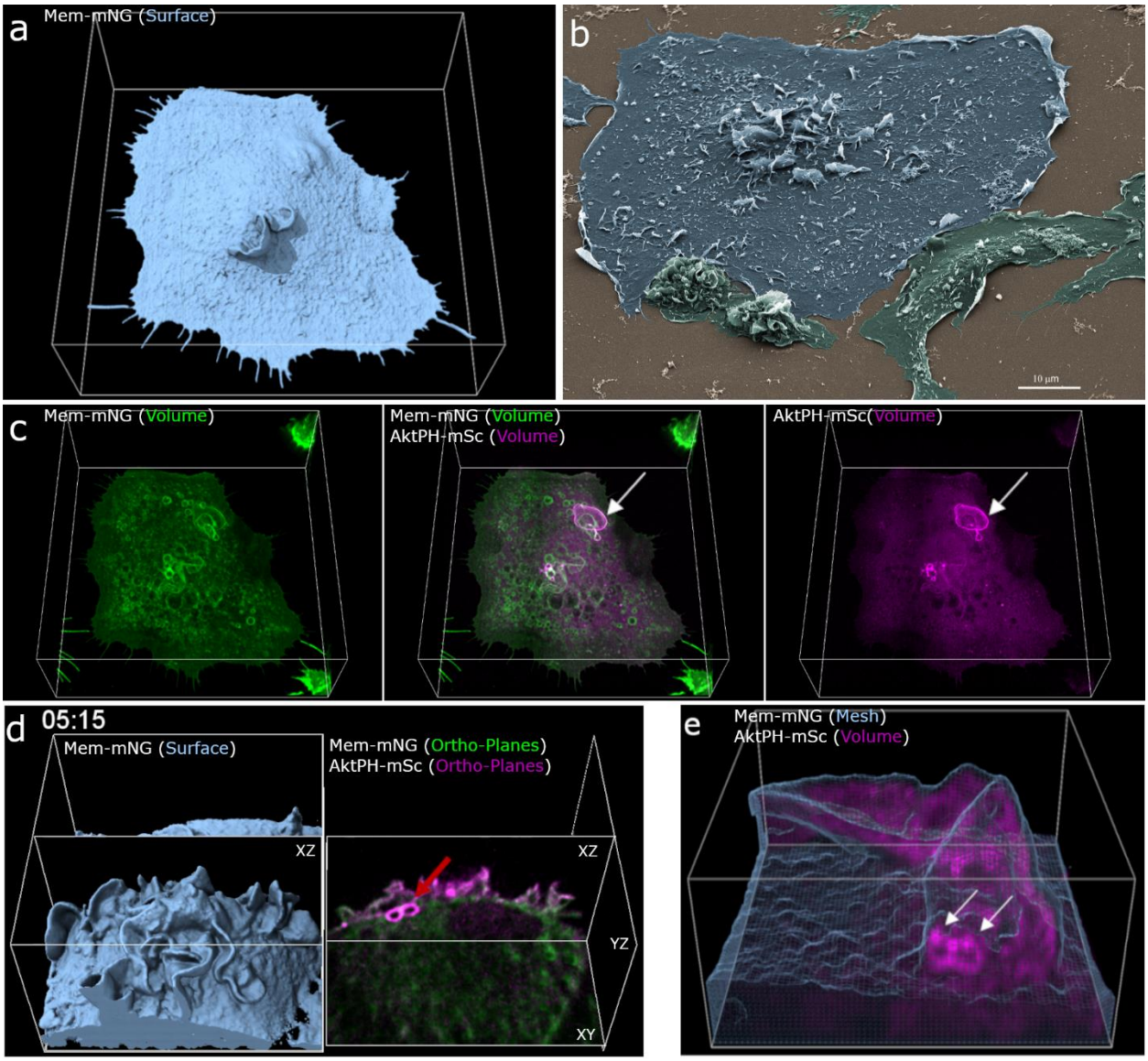

Figure 1. 3D visualization of macrophages allows insight into membrane structure and phosphatidylinositol dynamics during macropinocytosis. a) Isosurfaces show the plasma membrane of a live cell that is actively macropinocytosing (Region 68x72x25 µm x, y, z). b) SEM image of a macrophage acutely stimulated with CSF-1 shows high-resolution fixed cells (Scale bar is 10 µm) c) Volumetric intensities show specific local fluorescence (left->right) volumetric membrane (green), dual volumetric membrane and AktPH-mSc, volumetric AktPH-mSc (magenta). Volumetric renderings provide a method to visualize the transient fluorescent intensities throughout the volume of the cell (Region 68x72x25 µm). d) Combinations of visualization techniques such as Isosurface (left) displayed alongside orthogonal planes (right) further clarify how each plane is chosen to show internal intensities (Region 29x30x19 µm). e) Mesh rendering of the Mem-mNG probe along with volumetric AktPH-mSc provides a representation of the plasma membrane structure as well as underlying fluorescence. The white arrows indicate the post closure recruitment of AktPH-mSc (Region 13x14x7 µm). Different rendering methods provide insight into cellular characteristics such as structure, depth, and fluorescent intensity and provide a foundation for visualizing localization of AktPH-mSc to the constantly changing plasma membrane during macropinocytosis.

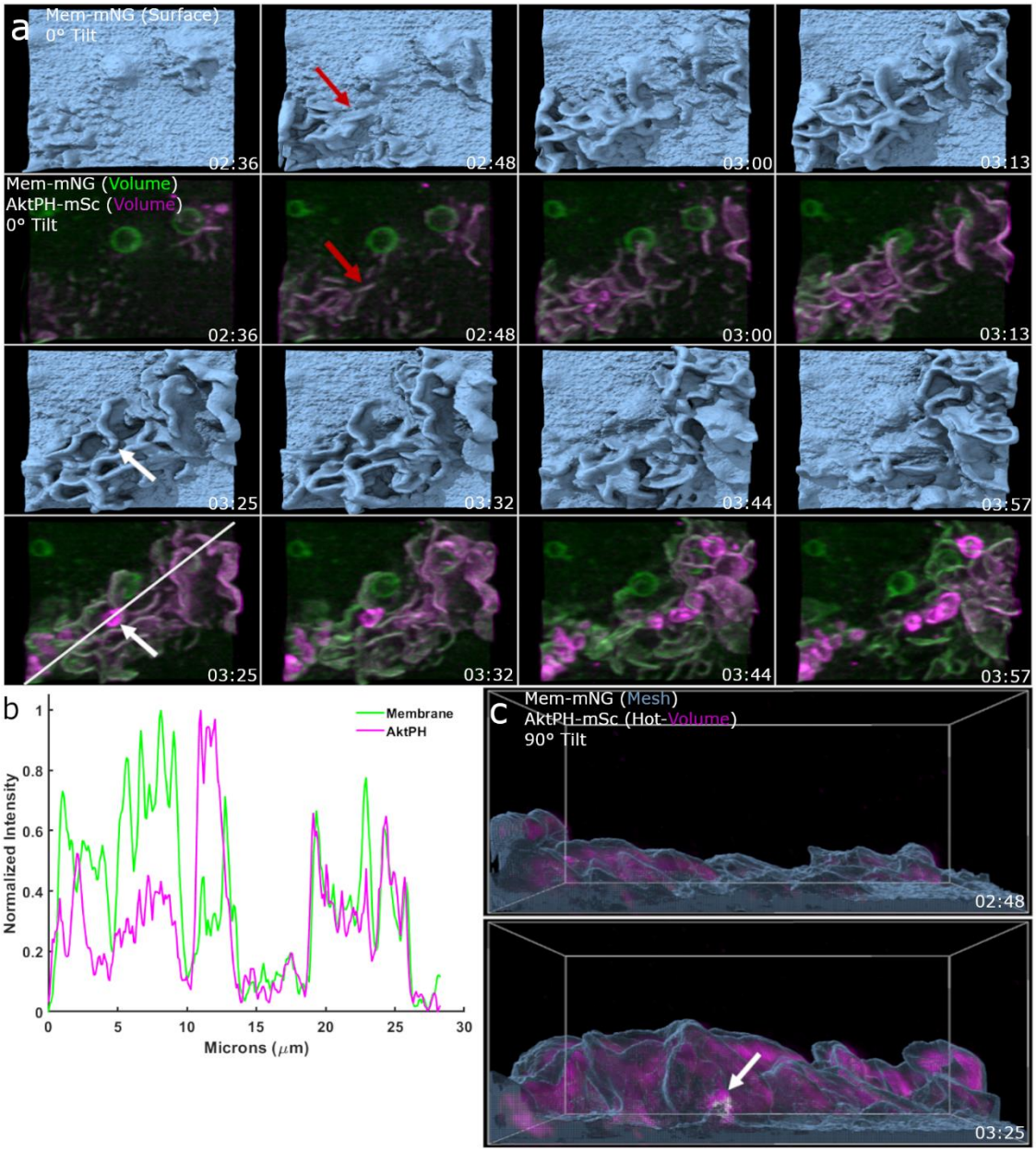

Figure 2. Early PI3K activity leads to amplification of PIP_3/PIP_2 in developing ruffles, macropinosome formation, and post closure recruitment. a) Top view of an Mem-mNG isosurface rendering provides depth for 3D visualization of ruffle extension. Dual-color volumetric intensity display comparing the recruitment of AktPH-mSc to early and expanding ruffles as well as sealed macropinosomes (Region 21x19um x,y). b) Intensity line-scan of the volumetric Mem-mNG and AktPH-mSc shows their co-scaled relative intensities for extending membrane ruffles, as well as recruitment around a sealed macropinosome. c) Side view of the isosurface mesh plasma membrane and volumetric AktPH-mSc (Magenta Hot color scale) from a shows that the early stages of ruffle development is filled with AktPH-mSc and the resulting macropinosome (white arrow) receives a final intense AktPH-mSc recruitment around the formed macropinosome at the bottom of the ruffle (Region 21x19x15um).

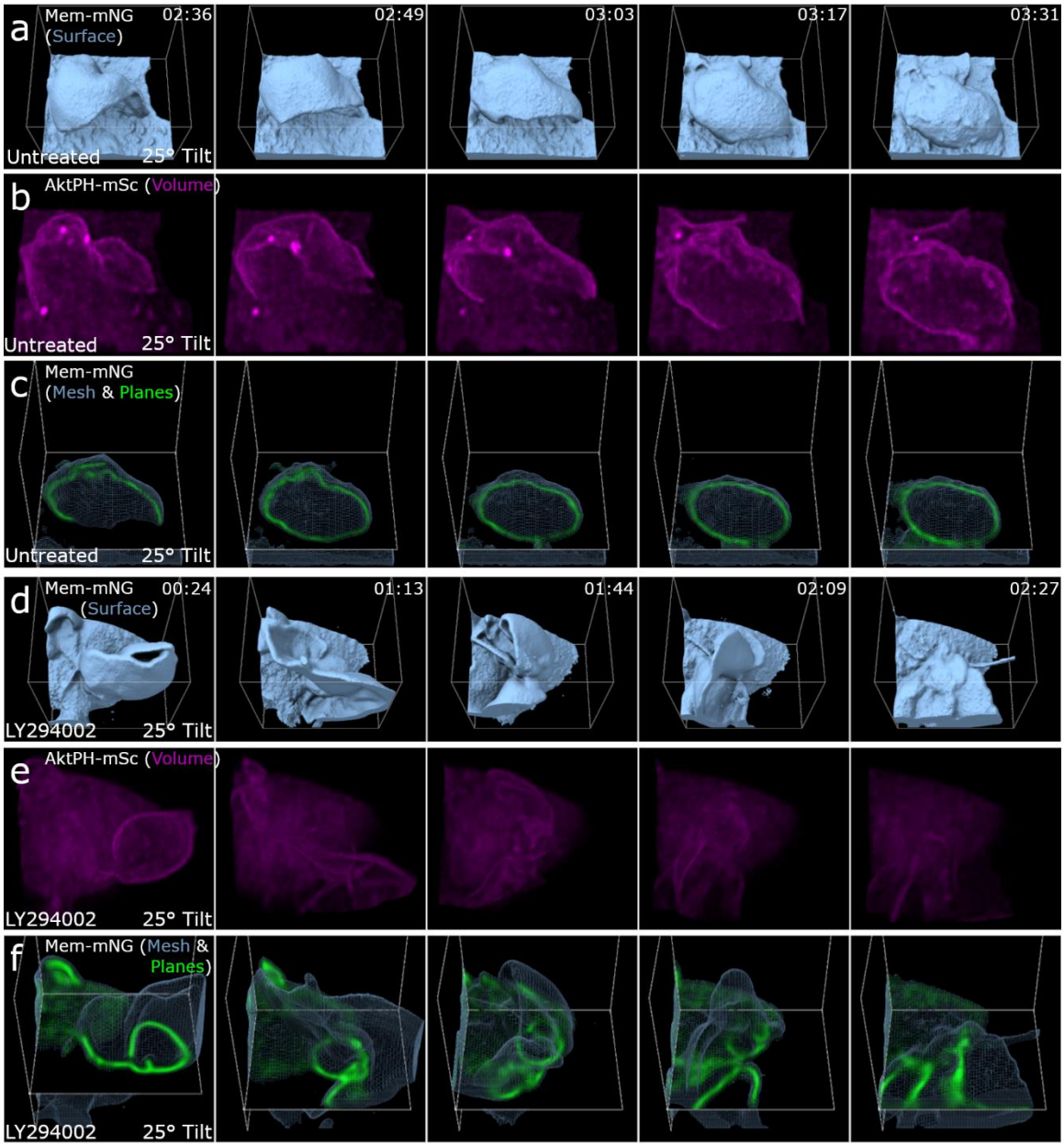

Figure 3. PI3K activity is required for membrane sealing and separation from PM/internalization of a complete macropinosome but not membrane ruffling a) Isosurface rendering of Mem-mNG for an untreated macrophage during a successful macropinocytosis event where the sheet curls back toward the membrane for fusion/sealing (Region 12x13x10 µm). b) Volumetric rendering of Sc-AktPH of the untreated cell shows the increase of PI3K activity in the ruffle that creates a macropinosome (Region 12x13x10 µm). c) Mesh and orthogonal planes of Mem-mNG show the internal membrane organization of the ruffle and resulting macropinosome (Region 12x13x10 µm). d) Isosurface rendering of an LY294002 treated macrophage provides depth to the attempted closure of a macropinocytic cup (Region 10x12x10 µm). e) Volumetric intensity rendering of Sc-AktPH for an LY294002-treated macrophage shows the diffuse distribution of AktPH and minimal PI3K activity. The cytosolic intensities were co-scaled for the untreated and treated macrophage (Region 10x12x10 µm). f) XY-plane for the Mem-mNG probe of an LY294002-treated cell during a failed macropinocytosis event. In the surface view, the ruffle appeared to form a macropinosome; however, when overlaid with the plane view is became clear that it failed to fully form into a macropinosome. The ruffle quickly reduced in size and became undistinguishable within the cytosol, while never receiving the post closure increase of PI3K activity (Region 10x12x10 µm).

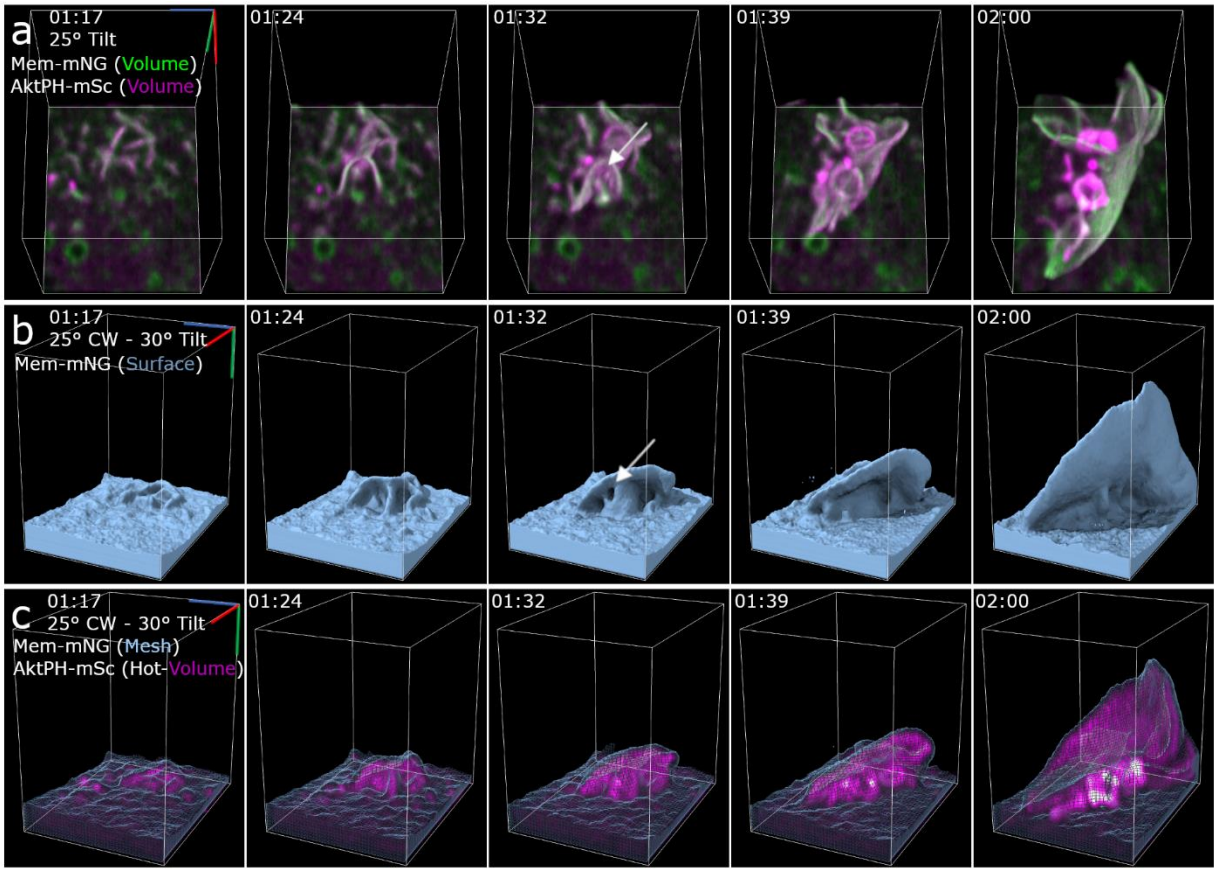

Figure 4. Macropinosomes form via PI3K-primed ruffle fusion. a) Dual volumetric intensities of Mem-mNG and AktPH-mSc show the intensity of each probe as the ruffles and macropinosomes form. The montage shows the earliest stage of the ruffle that extends vertically and forms macropinosomes along the length near the base of the primary ruffle as a result of smaller AktPH-mSc-rich extensions colliding. The white arrow points at the macropinosome forming region further emphasized in the isosurface (Region 9x12x13 µm). b) Isosurface rendering of Mem-mNG shows the structure of the extending ruffle and the continued sheet extension after the macropinosomes formed. The white arrow emphasizes the small pocket that closes to form one of the macropinosomes (Region 9x12x13 µm). c) Mesh surface rendering of Mem-mNG and volumetric AktPH-mSc shows the internalized macropinosome with the increased localization of AktPH-mSc at the bottom of the ruffle (Region 11x9x12 µm).

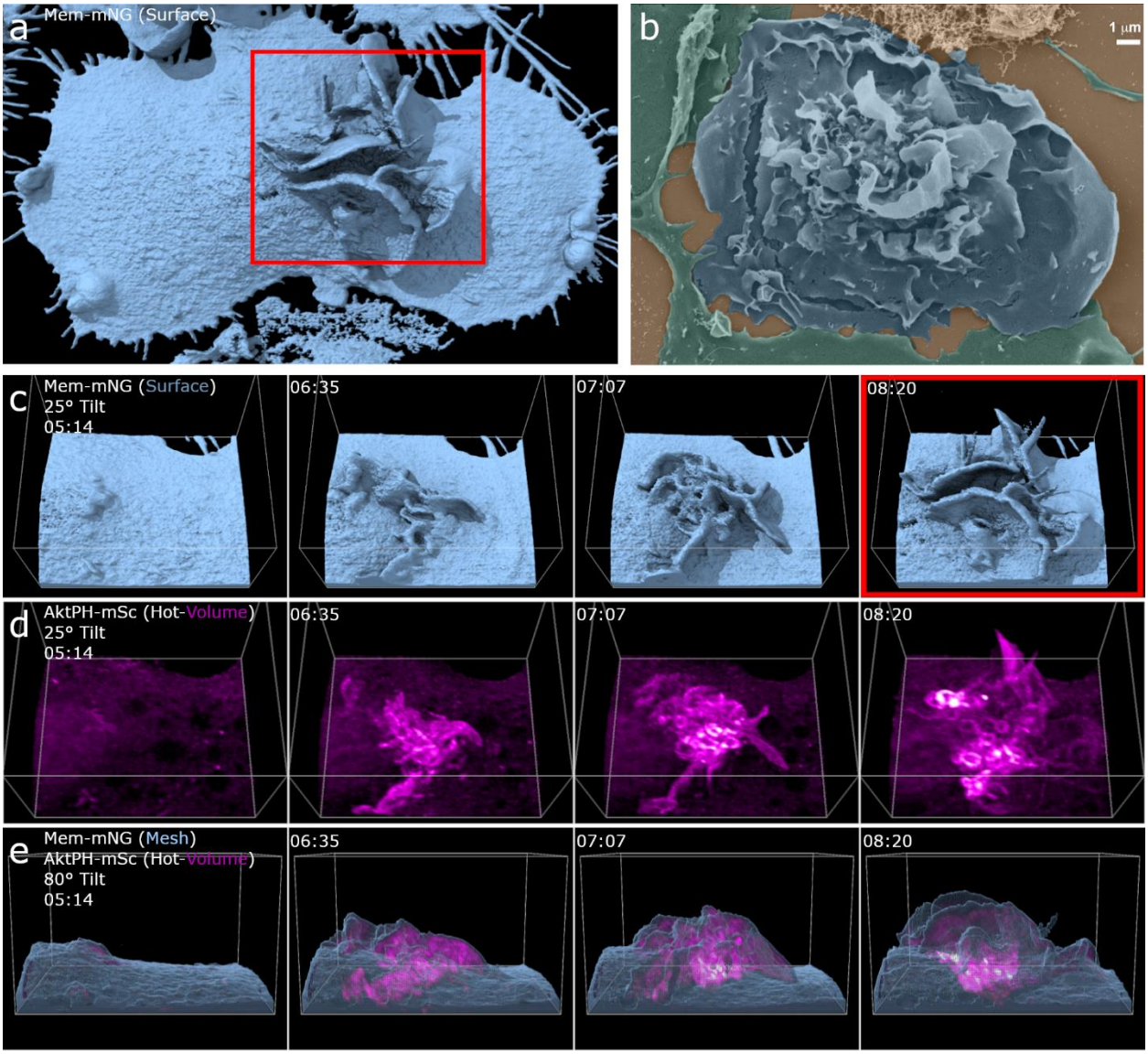

Figure 5. Phosphatidylinositol localization and chaotic ruffling underlie macropinocytosis in complex membrane structures. a) Single time point, full cell surface rendering of chaotic macropinocytosis event. The red box correlates to the same frame in c-d. b) SEM images of a BMDM showing similar highly active ruffling regions. Scale bar 1 µm c) Isosurface montage shows the chaotic orientation of membrane structure (Region 27x22x16 µm, 25° tilt). d) Volumetric AktPH-mSc (Magenta-Hot) provides a more detailed emphasis on the AktPH activity within the membrane ruffles and highlights the macropinosomes that have formed (Region 27x22x16 µm, 25° tilted). e) Mesh Surface with AktPH-mSc (Magenta Hot) shows the AktPH activity as the ruffle develops as well as the increased recruitment around formed macropinosomes at the base of the event.

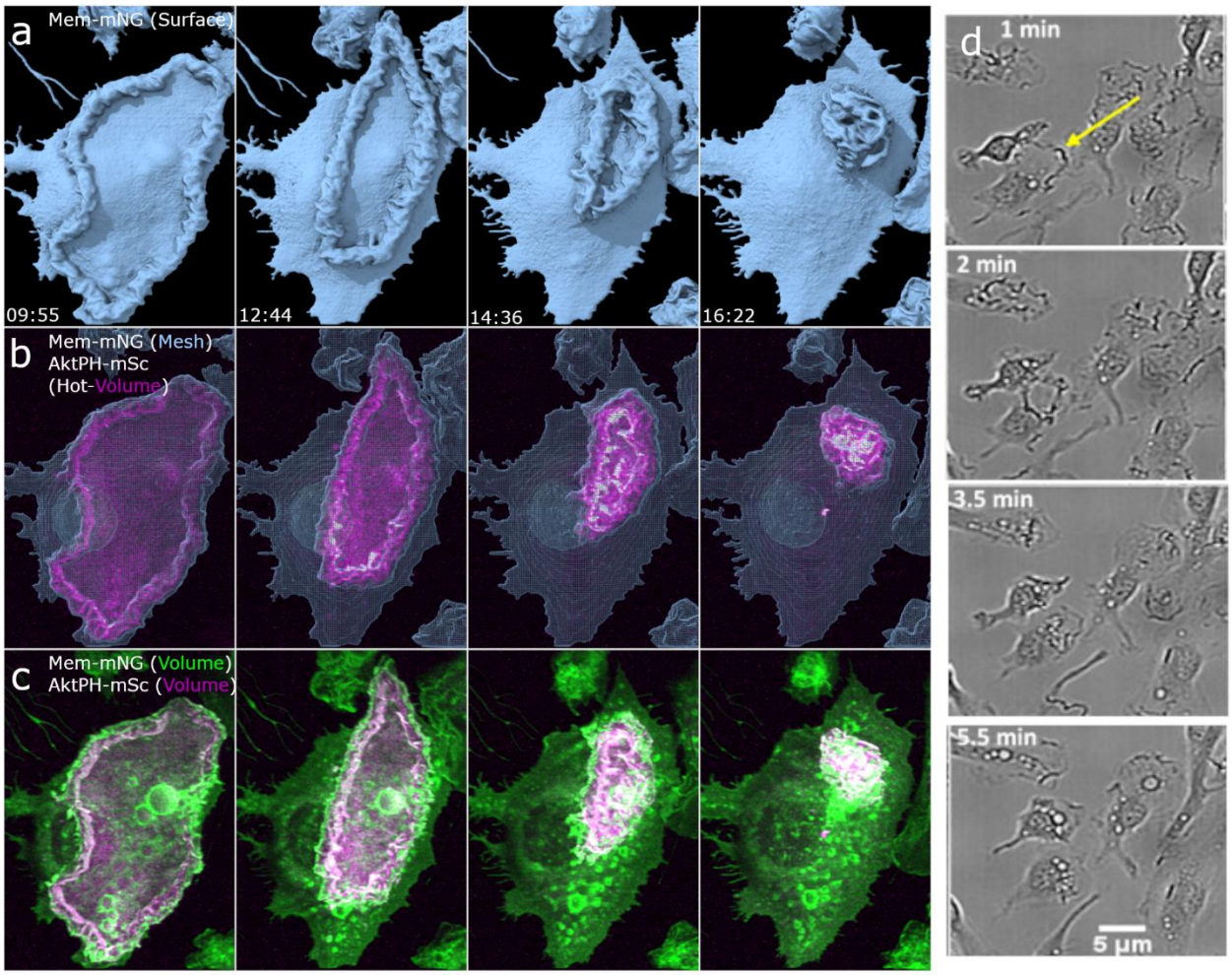

Figure 6. Growth factor starvation and stimulation results in the formation of large circular dorsal ruffles that corrals PIP_3/PIP_2. Macrophages were starved of CSF-1 for 24 h, imaged for 5 minutes as a baseline, and imaging restarted 1 min after stimulation with CSF-1. Four-frame montages provide a visual display of the large dorsal ruffle that acts as a diffusional barrier that restricts PIP_3/PIP_2 to the inside of the ruffle as it is cleared from the surface. This barrier is likely acting as a signal amplification mechanism stimulating the production of many macropinosomes. a) Isosurface rendering provides crisp surface directionality, b) Surface mesh and volumetric AktPH-mSc (magenta-hot), show the restricted probe as the membrane converges c) Volumetric Intensity of both Mem-mNG and AktPH-mSc show the intensity locations of the membrane ruffle and the restricted AktPH (49x60 µm x,y). d) Bright field images showing multiple cells responding to stimulation with similar dorsal membrane clearing.

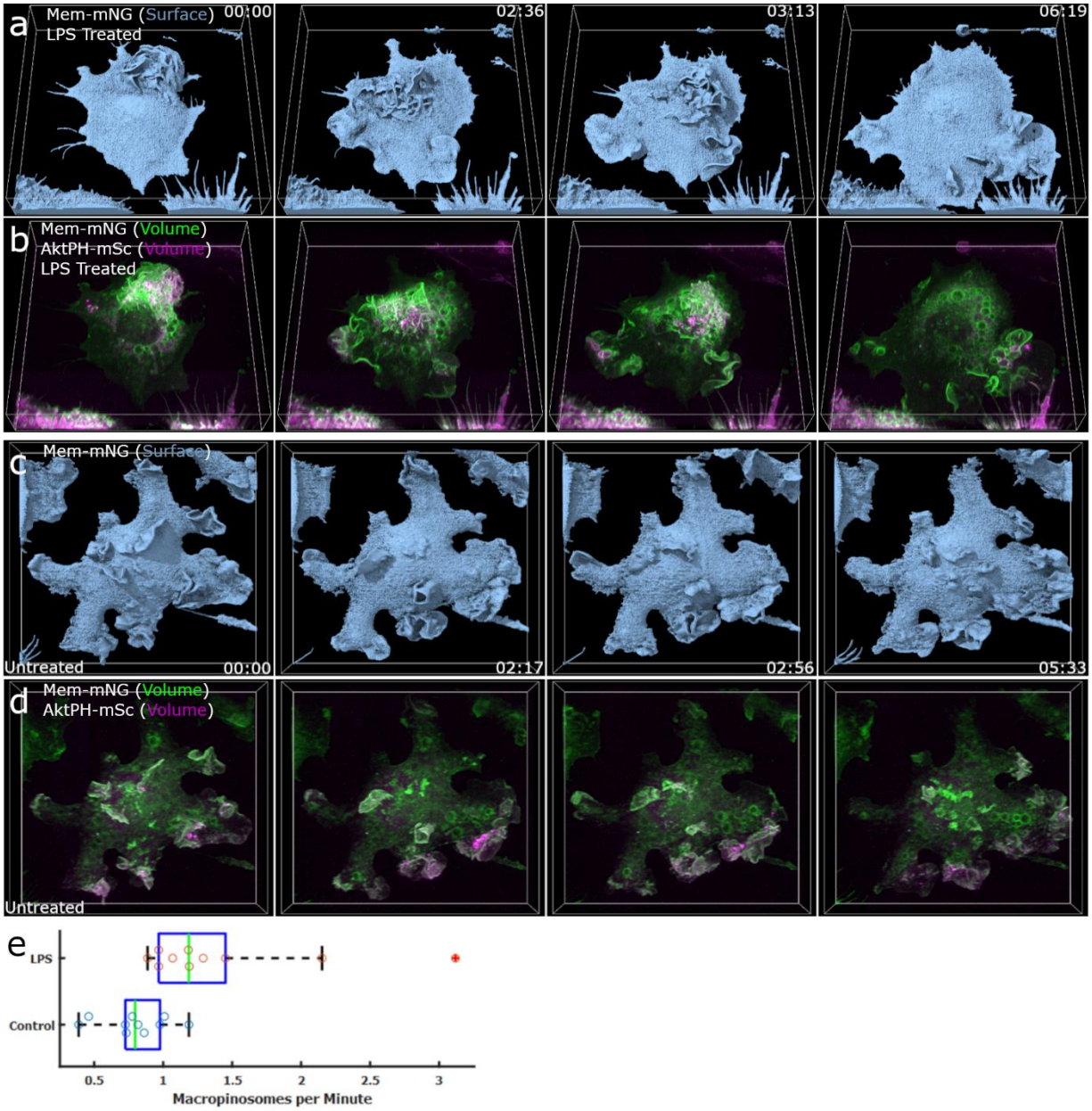

Figure 7. LPS stimulation increases membrane ruffling and macropinocytosis. Macrophages were pretreated with 100 ng·ml^{-1} LPS for 24 h prior to imaging. a) Surface rendering of Mem-mNG on an LPS stimulated macrophage provides a surface level understanding of the membrane, exploration, ruffling, and PM structure (Region 68x69x16 µm). b) Dual-color volumetric intensity projections of Mem-mNG and AktPH-mSc for an LPS stimulated cell provided the intensity activity during increased macrophage activity and shows the highly AktPH rich regions of membrane ruffling (Region 68x69x16 µm). c) Untreated macrophage Isosurface displaying less exploratory behavior (Region 68x64x16 µm). d) Dual-color volumetric intensity rendering of the untreated macrophage gives insight on the AktPH activity inside of the cell during macropinocytosis and allows for the quantitative comparison of macropinosomes formed between the stimulated and unstimulated cells (Region 68x64x16 µm). e) Box plot showing the difference in macropinocytic activity between untreated and LPS treated macrophages. All macropinosomes greater than 1 µm were manually counted using a z-projection MIP in Fiji and were distinguished by the post closure spike in AktPH-mSc intensity.

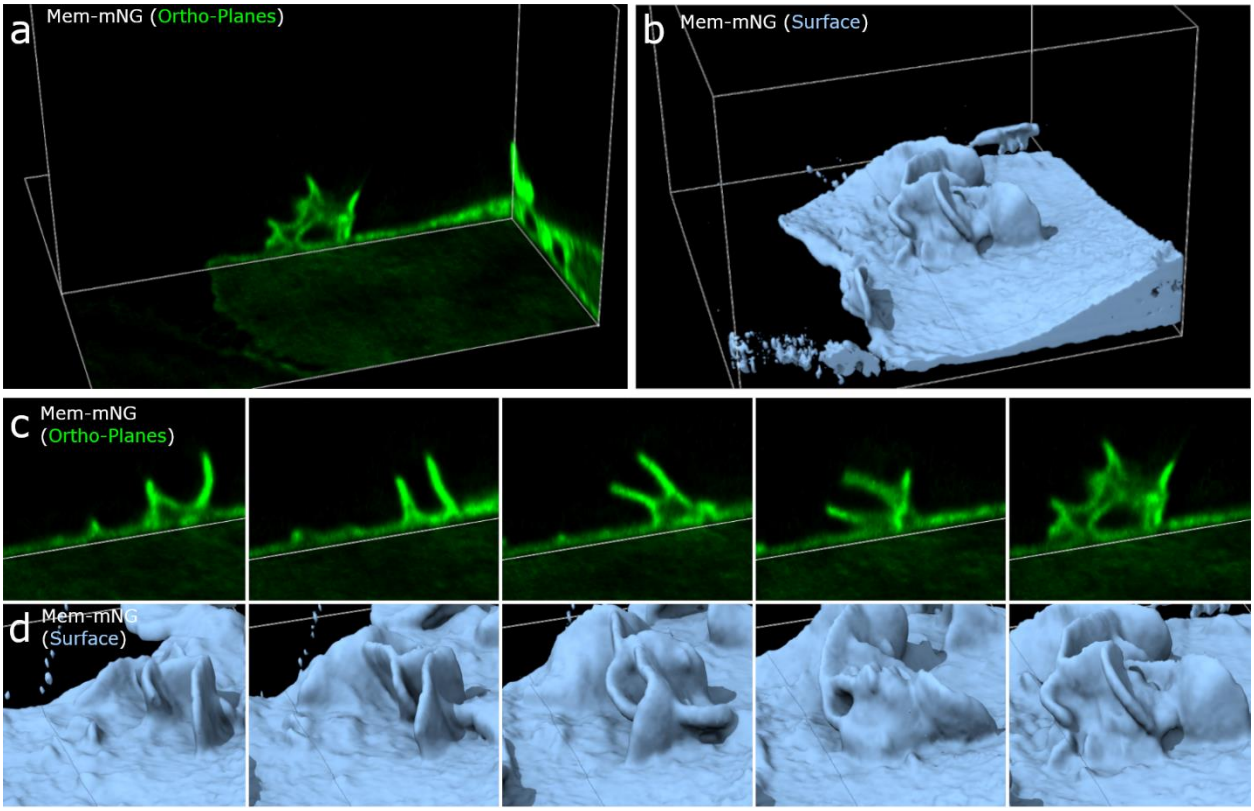

Supplementary Figure 1. Constitutive macropinocytosis and the importance of reducing the dimensionality of data. a) Orthoplane (left) and isosurface (right) views of Mem-mNG show the subsurface macropinosome and the complex structure of the full surface (Region 20x20x15 µm). b) Orthoplane montage of Mem-mNG depicting constitutive planar view of macropinocytosis where two ruffles extend from the cell membrane, circularize, and connect to form a macropinosome. c) Close view of the respective orthoplane and isosurface views of Mem-mNG showing the complex structures and the multiple membrane ruffles involved in the macropinocytic event.

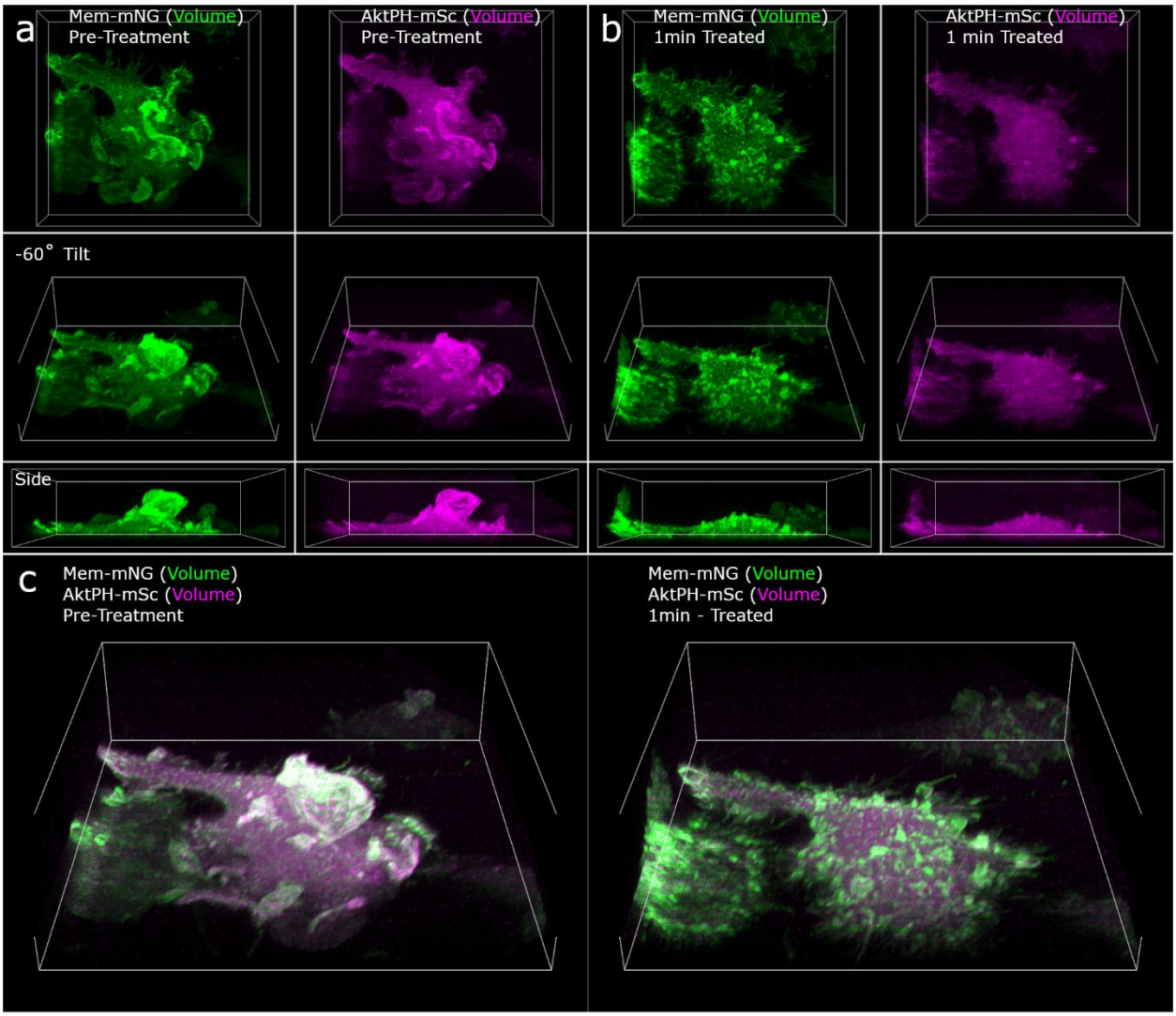

Supplementary Figure 2. LY294002 drug treatment response. a) Two columns showing different angles of a split volume representations for Mem-mNG and AktPH-mSc of an untreated macrophage actively ruffling and creating macropinosomes (Region 71x69x20 µm). b) Two columns showing the same cell treated with LY294002 displayed as split volumes of Mem-mNG and AktPH-mSc one minute after drug treatment (Region 71x69x20 µm). c) Composite volume representations of pre-treatment (left) and one minute post LY294002 drug treatment (right) (Region 71x69x20 µm).

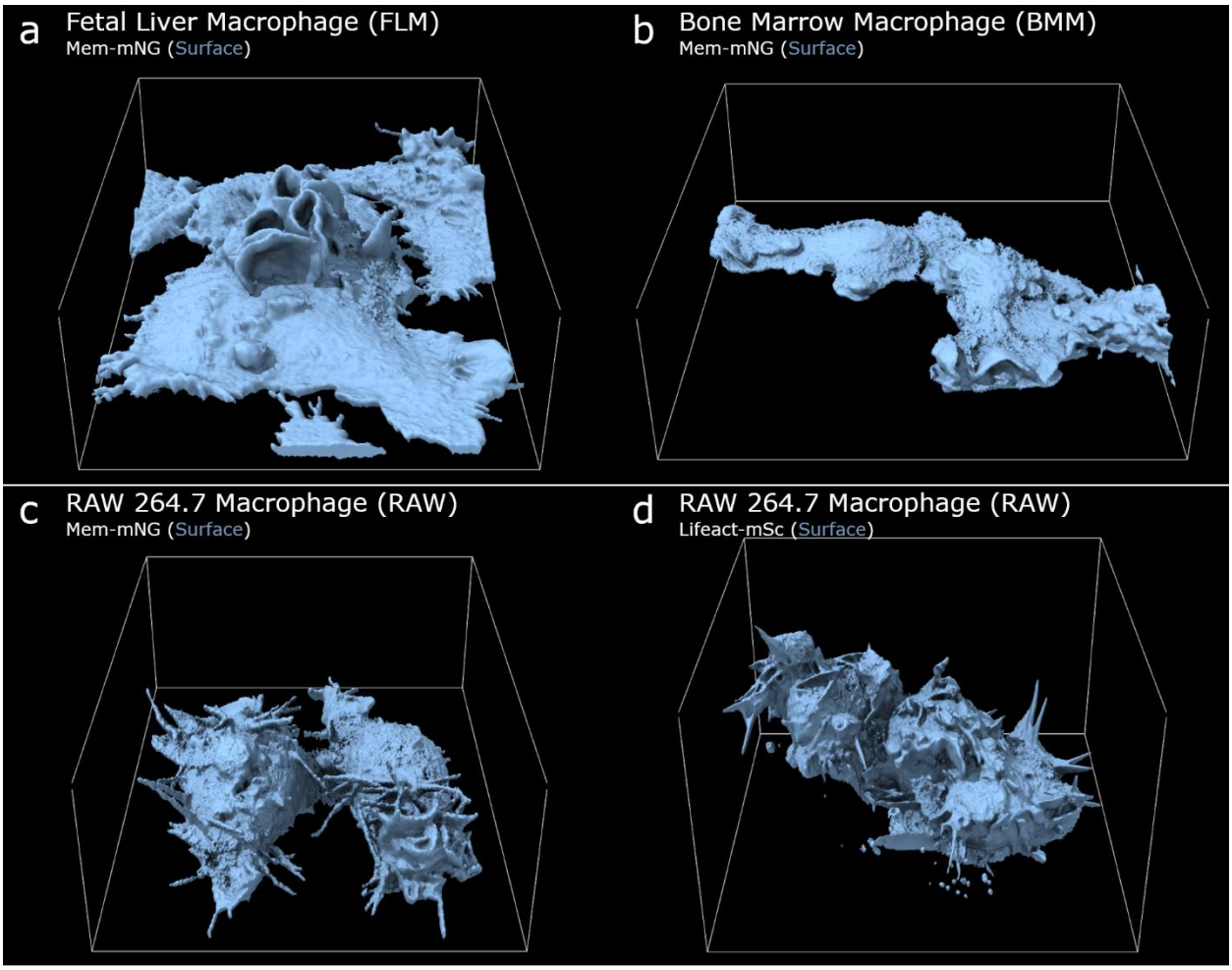

Supplementary Figure 3. Cell line variability and cross comparison. Isosurface view of Mem-mNG showing the general membrane structure observed by LLSM: a) fetal liver macrophage (Region 47x59x19 µm), b) bone marrow derived macrophage (Region 71x68x22 µm), and c) RAW264.7 (Region 50x38x17 µm). d) Isosurface view of Lifeact-mSc expressed in RAW264.7 demonstrating a similar morphology with filopodial extensions (Region 49x49x30 µm).

Supplementary Movie Legends

Video 1. Corresponds to Fig. 1a, c. Isosurface and volumetric intensity renderings (Green Mem-mNG; Magenta AktPH-mSc) provides different methods of visualizing the formation (surface) and trafficking of macropinosomes and AktPH-mSc accumulation (volume). Movie timestamps highlight the following events: AktPH enriched ruffle development (02:42), newly formed macropinosomes (06:29; 08:51; 10:58), and post closure AktPH recruitment (11:19). Frame rate of ~7s and each region is 68x72x25 µm.

Video 2. Corresponds to Fig. 1d. Isosurface rendering in conjunction with orthogonal planes moved through a volume provide ~0.1 µm thick planes to help visualize the internal and surface activity of Mem-mNG and AktPH-mSc including macropinosome closures (02:41; 05:15), membrane rich ruffles (00:00; 02:34; 05:08), previously formed internal macropinosomes (05:15 during scan), and mSc-Akt localization around a closed macropinosome (05:15 during scan). Framerate of ~7s and two subregions each 29x30x19 µm.

Video 3. Corresponds to Fig. 2a. Isosurface and dual-volumetric intensity projection of Mem-mNG and AktPH-mSc with a 25-degree tilt shows a variety of formation events. Several early formations occur prior to relaxation of the plasma membrane (01:58), followed by the development of another AktPH rich ruffle (02:48), membrane closure into a macropinosome (03:07 -> 3:13), and finally post closure recruitment of AktPH (03:25). Several macropinosomes form that are indicated by the recruitment of AktPH post closure (3:57; 07:16) and subsequently trafficked toward one another to merge (4:53; 05:18; 05:30; 07:54). Frame rate of ~6.25s and region of 21x19x15um.

Video 4. Corresponds to Fig. 2c. Mesh rendering of Mem-mNG and volumetric intensity projection of AktPH-mSc (Magenta-Hot) using a 90-degree tilt. The second play through contains a pause to emphasize the frame shown in Fig 2c and highlight the AktPH rich membrane ruffles (02:48) and the post closure recruitments (03:25; 03:57). Frame rate ~6.25s region of 21x19x15um.

Video 5. Corresponds to Fig. 3a, b. Isosurface in conjunction with three volumetric intensity renderings (Green Mem-mNG; Magenta AktPH-mSc) display a traditional formation in an untreated cell including the initial ruffle (00:00) that vertically extends and begins to form a tidal wave (01:31) back toward the surface of the cell, with membrane scission (03:24 -> 03:31) and finally the post closure recruitment for the largest macropinosome (08:07). Frame rate of 7s and Region of 12x13x10 µm.

Video 6. Corresponds to Fig. 3d, e. Isosurface with three volumetric intensity renderings (Green Mem-mNG; Magenta AktPH-mSc) on an LY294002 treated macrophage showing the initial ruffle with uniform AktPH throughout the cytosol and ruffle (00:00), attempted closure of the ruffle (00:30), continued compression of the attempted macropinosome (00:30 -> 02:27), becoming un-trackable within the cytosol with no AktPH recruitment to the attempted macropinosome. (Tracking done manually using orthogonal planes) Frame rate of 6.15s and Region 10x12x10 µm.

Video 7. Corresponds to Supplementary Figure 2 Two color volumetric intensity renderings (Green Mem-mNG; Magenta AktPH-mSc) showing a pre-treated macrophage creating large dorsal ruffles rich with PI3K activity. After ~9 minutes of imaging, the cells were introduced to LY294002 and the same cell was reimaged showing a rapid reduction in ruffling and PI3K activity. After ~9 minutes of treatment, we show a second cell showing the start of returning ruffle activity on the same coverslip. Finally, a third cell was imaged starting at ~18 minutes into drug treatment showing the return of moderate ruffle formations but no increased PI3K activity (Region 71x69x20 µm).

Video 8. Corresponds to Fig. 4a, b. Isosurface alongside three volumetric intensity renderings (Green Mem-mNG; Magenta AktPH-mSc) shows the formation of macropinosomes at the base of a larger ruffle. Membrane relaxes (00:56), small protrusions form with increased AktPH (01:17), two small ruffles, one in the back and one in the front mergers with the larger ruffle (01:32 -> 01:39) followed by post closure AktPH recruitment (01:53). Frame rate of 7s and region of 11x9x12 µm.

Video 9. Corresponds to Fig. 5c. Isosurface and dual-volumetric intensity projection of Mem-mNG and AktPH-mSc showing a smooth and relaxed membrane (00:00). A single macropinosome forms (05:06) followed by a large increased in membrane activity (06:35) resulting in a significant number of macropinosomes, indicated by the post closure AktPH recruitment, that turns into the chaotic membrane structure (06:35 -> 13:18). Frame rate of 8s and region size of 27x22x16 µm.

Video 10. Corresponds to Fig. 5e. Side view of Mem-mNG isosurface and mesh membrane with volumetric AktPH (Magenta Hot) shows the continued AktPH localization within the extending membrane structure (06:35). Utilizing the Magenta-Hot LUT regions displaying in white represent the increase in AktPH post macropinosome closure signifying a formed macropinosome (05:55; 06:59; 08:12; 11:50). Frame rate of 8s and region size of 27x22x16 µm.

Video 11. Corresponds to Fig. 6a, b, c. CSF-1 starved macrophage displayed using Mem-mNG isosurface/mesh/volume and AktPH volumes as magenta-hot under the mesh and Magenta alongside the volume membrane. The macrophage was imaged 07:41 prior to stimulation and reimaged one minute after CSF-1 stimulation (08:41) providing time to ensure instrument and imaging conditions had not changed. The starved cell ruffled and formed macropinosomes similar to the conventional cells (00:06; 01:46; 03:26) and upon stimulation (08:41) a large circular dorsal ruffle forms corralling the AktPH to one concentrated spot in the cell (16:22). Frame rate of 6.25s and region size of 49x60 µm.

Video 12. Corresponds to Fig. 6d. The brightfield view starts promptly after stimulation showing the majority of macrophages performing the similar dorsal membrane clearing seen in the LLSM imaging.

Video 13. Corresponds to Fig. 7a, b. LPS Stimulation. Isosurface of Mem-mNG and dual-color volumetric intensity projections of Mem-mNG and AktPH-mSc showing the activity of an LPS treated cell. Initial imaging starts (00:00) with a cluster of membrane rich in AktPH that goes on to create many macropinosomes as it expands toward the upper right region of the field of view. The activity changes directions toward the upper left region of the cell and proceeds to move counterclockwise (01:14), over the nucleus and back to the initial location ending at (04:42). Additional macropinosomes are seen forming on the left region with the increased AktPH flare up post closure (04:42). Finally, several formations occur in the bottom right of the cell (05:05 – 08:18) many of which go on to merge with one another. Framerate of ~7s and Region of 68x77x21 µm.

Video 14. Corresponds to Fig. 7c, d. Non-treated control. Isosurface of Mem-mNG and dual-color volumetric intensity projections of Mem-mNG and AktPH-mSc showing the imaging of a nontreated cell (10:47). Two AktPH rich regions of membrane ruffling are seen in the bottom right of the cell (02:17) that form several small macropinosomes, indicated by a spike in AktPH around the formed macropinosome. The cell shows activity that is representative of the untreated experiments including macropinosome formations, exploration, and overall membrane ruffling. Framerate of ~6.5s and Region of 68x77x21 µm.

Video 15. Corresponds to Supplementary Figure 3b. Isosurface rendering of Mem-mNG in a BMM. The cell shows activity that is representative of the BMM population including macropinosome formations, surface spreading, and overall membrane ruffling. Framerate of ~4.2s and region 71x68x22 µm).

Video 16. Corresponds to Supplementary Figure 3c. Isosurface rendering of Mem-mNG in an RAW264.7 cell. The cell shows activity that is representative of the RAW264.7 population including tentpole extensions, rounded shape, and general membrane activity. Framerate of ~3.5s and region 50x38x17 µm)**.**

References

1 Freeman, S. A. *et al.* Lipid-gated monovalent ion fluxes regulate endocytic traffic and support immune surveillance. *Science* **367**, 301-305, doi:10.1126/science.aaw9544 (2020).

2 Bohdanowicz, M. & Grinstein, S. Role of phospholipids in endocytosis, phagocytosis, and macropinocytosis. *Physiol Rev* **93**, 69-106, doi:10.1152/physrev.00002.2012 (2013).

3 Doodnauth, S. A., Grinstein, S. & Maxson, M. E. Constitutive and stimulated macropinocytosis in macrophages: roles in immunity and in the pathogenesis of atherosclerosis. *Philosophical Transactions of the Royal Society B: Biological Sciences* **374**, 20180147, doi:doi:10.1098/rstb.2018.0147 (2019).

4 Kerr, M. C. & Teasdale, R. D. Defining Macropinocytosis. *Traffic* **10**, 364-371, doi:10.1111/j.1600-0854.2009.00878.x (2009).

5 Redka, D. y. S., Gütschow, M., Grinstein, S. & Canton, J. Differential ability of proinflammatory and anti-inflammatory macrophages to perform macropinocytosis. *Molecular Biology of the Cell* **29**, 53-65, doi:10.1091/mbc.E17-06-0419 (2018).

6 Egami, Y., Taguchi, T., Maekawa, M., Arai, H. & Araki, N. Small GTPases and phosphoinositides in the regulatory mechanisms of macropinosome formation and maturation. *Frontiers in Physiology* **5**, doi:10.3389/fphys.2014.00374 (2014).

7 Swanson, J. A. & Yoshida, S. Macropinosomes as units of signal transduction. *Philosophical Transactions of the Royal Society B: Biological Sciences* **374**, 20180157, doi:doi:10.1098/rstb.2018.0157 (2019).

8 Yoshida, S. *et al.* Differential signaling during macropinocytosis in response to M-CSF and PMA in macrophages. *Frontiers in physiology* **6**, 8-8, doi:10.3389/fphys.2015.00008 (2015).

9 Lou, J., Low-Nam, S., Kerkvliet, J. & Hoppe, A. Delivery of CSF-1R to the lumen of macropinosomes promotes its destruction in macrophages. *Journal of cell science* **127**, doi:10.1242/jcs.154393 (2014).

10 Bloomfield, G. & Kay, R. R. Uses and abuses of macropinocytosis. *Journal of Cell Science* **129**, 2697, doi:10.1242/jcs.176149 (2016).

11 Pacitto, R., Gaeta, I., Swanson, J. A. & Yoshida, S. CXCL12-induced macropinocytosis modulates two distinct pathways to activate mTORC1 in macrophages. *Journal of Leukocyte Biology* **101**, 683-692, doi:https://doi.org/10.1189/jlb.2A0316-141RR (2017).

12 Condon, N. D. *et al.* Macropinosome formation by tent pole ruffling in macrophages. *Journal of Cell Biology* **217**, 3873-3885, doi:10.1083/jcb.201804137 (2018).

13 Swanson, J. A. Shaping cups into phagosomes and macropinosomes. *Nature Reviews Molecular Cell Biology* **9**, 639-649, doi:10.1038/nrm2447 (2008).

14 Botelho, R. J. *et al.* Localized Biphasic Changes in Phosphatidylinositol-4,5-Bisphosphate at Sites of Phagocytosis. *Journal of Cell Biology* **151**, 1353-1368, doi:10.1083/jcb.151.7.1353 (2000).

15 Freeman, S. A. & Grinstein, S. Phagocytosis: receptors, signal integration, and the cytoskeleton. *Immunol Rev* **262**, 193-215, doi:10.1111/imr.12212 (2014).

16 King, J. S. & Kay, R. R. The origins and evolution of macropinocytosis. *Philosophical Transactions of the Royal Society B: Biological Sciences* **374**, 20180158, doi:doi:10.1098/rstb.2018.0158 (2019).

17 Yoshida, S., Hoppe, A. D., Araki, N. & Swanson, J. A. Sequential signaling in plasma-membrane domains during macropinosome formation in macrophages. *Journal of Cell Science* **122**, 3250-3261, doi:10.1242/jcs.053207 (2009).

18 Veltman, D. M. *et al.* A plasma membrane template for macropinocytic cups. *eLife* **5**, e20085, doi:10.7554/eLife.20085 (2016).

19 Donaldson, J. G. Macropinosome formation, maturation and membrane recycling: lessons from clathrin-independent endosomal membrane systems. *Philosophical Transactions of the Royal Society B: Biological Sciences* **374**, 20180148, doi:doi:10.1098/rstb.2018.0148 (2019).

20 Maekawa, M. *et al.* Sequential breakdown of 3-phosphorylated phosphoinositides is essential for the completion of macropinocytosis. *Proceedings of the National Academy of Sciences* **111**, E978, doi:10.1073/pnas.1311029111 (2014).

21 Buckley, C. M. & King, J. S. Drinking problems: mechanisms of macropinosome formation and maturation. *The FEBS Journal* **284**, 3778-3790, doi:10.1111/febs.14115 (2017).

615 22 Araki, N., Egami, Y., Watanabe, Y. & Hatae, T. Phosphoinositide metabolism during membrane ruffling and
616 macropinosome formation in EGF-stimulated A431 cells. *Exp Cell Res* **313**, 1496-1507,
617 doi:10.1016/j.yexcr.2007.02.012 (2007).
618 23 Welliver, T. P. & Swanson, J. A. A growth factor signaling cascade confined to circular ruffles in
619 macrophages. *Biology Open* **1**, 754, doi:10.1242/bio.20121784 (2012).
620 24 Chamberlain, L. M., Godek, M. L., Gonzalez-Juarrero, M. & Grainger, D. W. Phenotypic non-equivalence of
621 murine (monocyte-) macrophage cells in biomaterial and inflammatory models. *Journal of Biomedical*
622 *Materials Research Part A* **88A**, 858-871, doi:https://doi.org/10.1002/jbm.a.31930 (2009).
623 25 Gao, L., Shao, L., Chen, B.-C. & Betzig, E. 3D live fluorescence imaging of cellular dynamics using Bessel
624 beam plane illumination microscopy. *Nature Protocols* **9**, 1083-1101, doi:10.1038/nprot.2014.087 (2014).
625 26 Goddard, T. D. *et al.* UCSF ChimeraX: Meeting modern challenges in visualization and analysis. *Protein Sci*
626 **27**, 14-25, doi:10.1002/pro.3235 (2018).
627 27 Araki, N., Johnson, M. T. & Swanson, J. A. A role for phosphoinositide 3-kinase in the completion of
628 macropinocytosis and phagocytosis by macrophages. *Journal of Cell Biology* **135**, 1249-1260,
629 doi:10.1083/jcb.135.5.1249 (1996).
630 28 Luyendyk, J. P. *et al.* Genetic Analysis of the Role of the PI3K-Akt Pathway in Lipopolysaccharide-Induced
631 Cytokine and Tissue Factor Gene Expression in Monocytes/Macrophages. *The Journal of Immunology* **180**,
632 4218-4226, doi:10.4049/jimmunol.180.6.4218 (2008).
633 29 Hoeller, O. *et al.* Two distinct functions for PI3-kinases in macropinocytosis. *Journal of Cell Science* **126**,
634 4296, doi:10.1242/jcs.134015 (2013).
635 30 Hacker, U., Albrecht, R. & Maniak, M. Fluid-phase uptake by macropinocytosis in Dictyostelium. *Journal of*
636 *Cell Science* **110**, 105-112, doi:10.1242/jcs.110.2.105 (1997).
637 31 Williams, T. D., Peak-Chew, S.-Y., Paschke, P. & Kay, R. R. Akt and SGK protein kinases are required for
638 efficient feeding by macropinocytosis. *Journal of Cell Science* **132**, doi:10.1242/jcs.224998 (2019).
639 32 Stewart, S. A. *et al.* Lentivirus-delivered stable gene silencing by RNAi in primary cells. *Rna* **9**, 493-501,
640 doi:10.1261/rna.2192803 (2003).
641 33 Sancak, Y. *et al.* The Rag GTPases bind raptor and mediate amino acid signaling to mTORC1. *Science* **320**,
642 1496-1501, doi:10.1126/science.1157535 (2008).
643 34 Chertkova, A. O. *et al.* Robust and Bright Genetically Encoded Fluorescent Markers for Highlighting
644 Structures and Compartments in Mammalian Cells. *bioRxiv*, 160374, doi:10.1101/160374 (2020).
645 35 Fejer, G. *et al.* Nontransformed, GM-CSF–dependent macrophage lines are a unique model to study tissue
646 macrophage functions. *Proceedings of the National Academy of Sciences* **110**, E2191-E2198,
647 doi:10.1073/pnas.1302877110 (2013).
648 36 Lebedev, M., Swaminathan, P., Kerkvlie, J. G., Hoppe, A. D. & Thiex, N. Immortal fetal liver macrophages
649 as a new model for studying macrophage function. *Molecular Biology of the Cell* **27** (2016).
650 37 Stanley, E. R., Cifone, M., Heard, P. M. & Defendi, V. Factors regulating macrophage production and
651 growth: identity of colony-stimulating factor and macrophage growth factor. *J Exp Med* **143**, 631-647,
652 doi:10.1084/jem.143.3.631 (1976).
653 38 Waheed, A. & Shadduck, R. K. Purification and properties of L cell-derived colony-stimulating factor. *J Lab*
654 *Clin Med* **94**, 180-193 (1979).
655 39 tlambert03/LLSpy: v0.4.8 v. 0.4.8 (Zenodo, 2019).
656